

OH-initiated oxidation of benzene

Part I. Phenol formation under atmospheric conditions

Rainer Volkamer,^{*ab} Björn Klotz,^{cd} Ian Barnes,^d Takashi Imamura,^c Klaus Wirtz,^b
Nobuaki Washida,^e Karl Heinz Becker^d and Ulrich Platt^a

^a Universität Heidelberg, Institut für Umweltphysik, Im Neuenheimer Feld 229, D-69120 Heidelberg, Germany. E-mail: rainer.volkamer@iup.uni-heidelberg.de; Fax: +49 6221 54 6405; Tel: +49 6221 54 6527

^b Fundación CEAM, Parque Tecnológico, Calle Charles R. Darwin 14, E-46980 Paterna (Valencia), Spain

^c National Institute for Environmental Studies, Atmospheric Environment Division, 16-2 Onogawa, Tsukuba-shi, Ibaraki-ken 305-8506, Japan

^d Bergische Universität Wuppertal, Physikalische Chemie-FB 9, Gaußstraße 20, D-42097 Wuppertal, Germany

^e Kyoto University, Department of Chemistry, Graduate School of Science, Sakyo-ku, Kyoto 606-8502, Japan

Received 26th September 2001, Accepted 15th January 2002

First published as an Advance Article on the web 21st March 2002

The phenol yield from the OH-radical initiated oxidation of benzene was studied in two simulation chambers: (1) the large-volume outdoor chamber EUPHORE at CEAM, Valencia, Spain and (2) an indoor chamber at NIES, Tsukuba, Japan. In the first study two spectroscopic techniques, *i.e.* differential optical absorption spectroscopy (DOAS) and Fourier transform infra-red spectroscopy (FTIR) were used to simultaneously measure phenol and benzene. The second study used only FTIR spectroscopy to monitor both compounds. Six different types of OH-radical sources were employed and initial concentrations for benzene and NO_x were varied by about a factor of 400 and four orders of magnitude, respectively. The high sensitivity of DOAS towards phenol allowed experiments with initial benzene concentrations similar to those found in the polluted atmosphere. With respect to the NO_x concentrations and light conditions employed, the experiments are representative of the atmospheric boundary layer. The phenol yield was determined to be $\Phi_{\text{phenol}} = (53.1 \pm 6.6)\%$, which is about twice the value reported in the literature to date. The high phenol yield was found to remain essentially constant for NO_x levels of up to several 10 ppb, which are rarely exceeded in the atmosphere. It was also found to be independent of the oxygen concentration under these conditions. With increasing concentrations of NO_x (> 100 ppb) the phenol yield was found to decrease. The data could be adequately described if in addition to the kinetics of the aromatic-OH adduct reactions with O₂ two reactions involving NO_x (*i.e.* benzene-OH + NO₂ and benzene-OH-O₂ + NO) were considered. The temperature dependence of Φ_{phenol} was studied over a limited temperature range of $\Delta T = 20$ K. The results indicate that the major part, if not all of the phenol is formed directly from the reaction of the benzene-OH adduct with oxygen. No evidence was found for phenol formation *via* the photolysis of benzene oxide/oxepin. The atmospheric relevance of the results is discussed.

1. Introduction

Aromatic hydrocarbons are an abundant constituent of the urban atmosphere, with emissions coming mainly from road traffic and solvent use.¹⁻³ This class of hydrocarbons is assumed to be responsible for a significant fraction of the photo-oxidant formation in industrialised countries. Another aspect of the impact of aromatic hydrocarbons on the atmospheric environment is their effect on health. Benzene, for example, is carcinogenic and its use is therefore strictly controlled.⁴ In addition the photo-oxidation products of aromatic hydrocarbons are known to show both toxic and mutagenic effects, in contrast to those of most smaller alkenes and alkanes.⁵

Despite their importance the knowledge about the atmospheric degradation mechanisms of aromatic hydrocarbons,

in particular of benzene is still scant. Most experimental studies have focussed on the more reactive aromatic hydrocarbons like toluene and the xylene isomers. It is well established that benzene and the alkylated benzenes react almost exclusively with OH radicals under the conditions prevalent in the lower troposphere.⁶ Reactions with ozone, NO₃ radicals and other atmospheric oxidants and also photolysis are negligible in comparison. In spite of recent intensive research efforts considerable uncertainty still exists on the principal oxidation steps in the OH-radical degradation of aromatic compounds. One specific aspect of fundamental importance for mechanism development is the branching ratio between ring-fragmentation and ring-retention. It is known that ring-retaining products like phenol and benzaldehyde derivatives do not contribute as efficiently to photo-oxidant formation as the products formed after ring-fragmentation.

Also, the toxic effects of aromatic hydrocarbon photo-oxidation products are usually attributed to ring-fragmentation products.⁶

In the case of benzene studied here, there is an additional incentive to study the branching ratio between ring-fragmentation and ring-retention products. Various proposed mechanisms for the OH-initiated oxidation of this compound differ both in the predicted formation yield and in the formation mechanism of phenol. Fig. 1 illustrates the initial oxidation steps in the reaction of OH with benzene and includes the different mechanisms currently proposed for the formation of phenol. Because of the fact that benzene oxidation proceeds, in contrast to the alkylated aromatic hydrocarbons, exclusively through the addition pathway of the OH-radical to the aromatic ring an understanding of the initial steps of benzene oxidation is also of fundamental importance for alkyl aromatic hydrocarbons in general. The abstraction channel, which accounts for <10% of the OH reaction products of simple alkylated benzenes, is comparably well understood.⁶

It is well established that the reaction of the OH radical with benzene **1** proceeds by addition to the aromatic ring giving a hydroxycyclohexadienyl radical **2**, also termed benzene-OH adduct (reaction (1) in Fig. 1). The benzene-OH adduct **2** only slowly decomposes back to reactants (-1) under atmospheric conditions and reversibly adds molecular oxygen⁷ to form the hydroxycyclohexadienyl peroxy radical **3**, see reaction (2). With $k_2 \approx 2 \times 10^{-15} \text{ cm}^3 \text{ s}^{-1}$ and $k_{-2} \approx 8 \times 10^3 \text{ s}^{-1}$, the equilibrium between **2** and **3** is rapidly attained (<1 ms) and it is not yet possible to differentiate between the two radical species **2** and **3** with respect to the further loss processes.⁸ The reported equilibrium constant, $K_{\text{eq}} = k_2/k_{-2} = 2.7 \times 10^{-19} \text{ cm}^3$ at $T = 296 \text{ K}$,⁸ indicates that **2** and **3** are present at roughly equal concentration in air at one atmosphere. Both radicals may form in chemically activated states⁹ which for reasons of simplicity are not explicitly shown in Fig. 1.

With respect to the formation of phenol **4** from **2** and **3**, different pathways (3) to (6) and (10) have been proposed. Channel (3) in Fig. 1 forms HO₂ through a hydrogen abstraction reaction of **2** with molecular oxygen. Channel (4) in principle yields the same products through the direct elimination of HO₂ from **3**.⁹ The formation of phenol without involvement of O₂ has been proposed to proceed by elimination of a ring-

bound H atom from **2**, see reaction (5),¹⁰ and this pathway has been the topic of intensive discussion in the literature.^{8,11,12} Finally, another possible pathway, shown as (6), was proposed by Klotz *et al.*¹³ Reaction of the hydroxy cyclohexadienyl radical **2** with O₂ was proposed to yield an HO₂ radical and benzene oxide **5**, which is in rapid equilibrium with its monocyclic isomer oxepin **6**. Mixtures of benzene oxide/oxepin **5/6** have been shown to yield phenol on photolysis with sunlight, reaction (7) in Fig. 1, while its OH initiated oxidation gives ring-opening products.¹³

Reactions (8) to (12) have also been proposed as loss processes of the species **2** and **3**. Of these, channels (8) and (9) are thought to dominate under atmospheric conditions leading in part to epoxide-type compounds¹⁴ and further ring-cleavage products.^{6,15} Channel (10), the reaction of **2** with NO₂, can be important under (smog chamber) conditions with high NO₂ concentrations. This reaction has been proposed to lead, among other products, to the formation of phenol,¹⁶ though another study¹⁰ found no evidence for this. Channel (11), the reaction of NO with **2**, will be essentially negligible under most conditions.⁷ Finally, channel (12) indicates the reaction of intermediate **3** with NO. This process is negligible under atmospheric NO concentrations⁷ but it may become an important loss process for the equilibrium **2/3** under simulated atmospheric conditions if NO concentrations are fairly high.

In the scheme presented in Fig. 1, reactions (8) to (12) will compete with the phenol forming channels (3) to (6) and are expected to reduce the phenol yield under high NO_x concentrations. If on the other hand the NO_x concentration is low, the phenol yield essentially depends on the relative importance of channels (3) to (6) and (8) and (9). In the present study, information about the relative importance of these channels is obtained by varying the parameters OH-radical source, temperature, oxygen partial pressure and initial NO_x concentration in the OH-initiated oxidation of benzene.

2. Experimental

Experiments were performed in two facilities: the outdoor European Photo-Reactor (EUPHORE), located near Valencia, Spain and the indoor photo-reactor at the NIES, Tsukuba, Japan.

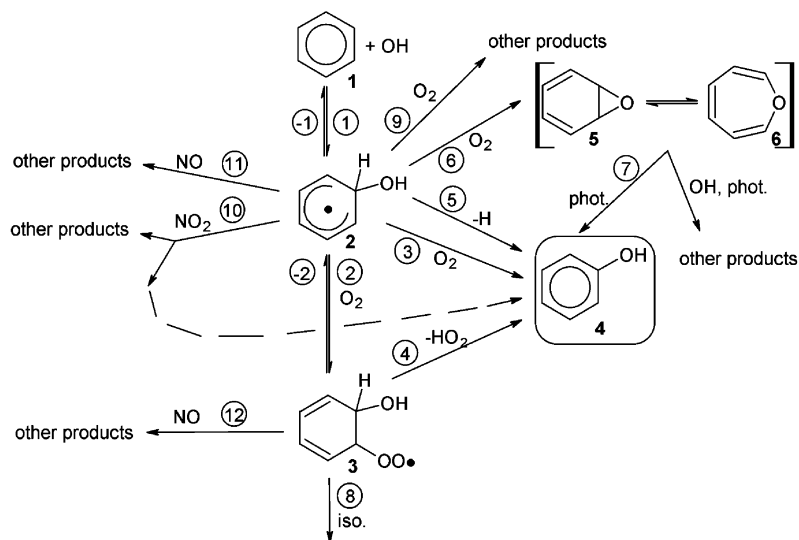


Fig. 1 The initial steps in the OH-initiated oxidation of benzene **1**. Currently proposed loss processes of the benzene-OH adduct **2** and the peroxy radical **3** (which are in a rapidly established equilibrium) are shown that lead in part to the formation of phenol **4**. Reaction pathways are indicated by numbers in circles and corresponding rate constants, if available, are given in the text.

2.1 EUPHORE

The EUPHORE installations, located at the CEAM institute in Valencia, Spain, consist of two hemispherical chambers made of 120 μm thick FEP foil, highly transparent for visible as well as UV light (transmittance in the visible is approximately 85–90%, at 290 nm about 75%). The chamber used in this study has an approximate volume of about 187 m^3 and a surface to volume ratio (S/V) of 0.7 m^{-1} . Detailed descriptions of the EUPHORE facilities are given in the literature.^{17,18}

UV enhanced aluminium coated mirrors (Alflex-UV, Balzers, Liechtenstein) were employed for the actively laser aligned White-system coupled to the DOAS (differential optical absorption spectroscopy). Spectra were recorded using 16 or 48 traverses corresponding to 130 m or 386 m absorption paths, respectively. A 500 W Xe-high pressure arc lamp (Professional Lamps INC, New Jersey, USA) was used as light source. The f/6.9 Czerny Turner spectrograph of the DOAS instrument (ACTON 500, focal length: 0.5 m) equipped with a linear photo-diode array detector (Hamamatsu, 1024 diodes, Hoffmann Messtechnik, Rauenberg) was operated at either (1) 0.2 nm (grating 1 : 1200 grooves mm^{-1} , blaze wavelength: 300 nm) or (2) 0.84 nm (grating 2 : 300 grooves mm^{-1} , blaze wavelength: 500 nm) spectral resolution (FWHM). Spectra were recorded in the spectral intervals (1) 250 nm to 290 nm or (2) 246 nm to 411.8 nm yielding a time resolution from a few seconds to less than 5 min.

The second White-system, coupled to the FTIR (Fourier transform infra-red) spectrometer was equipped with gold-coated mirrors and was operated at 40 traverses, corresponding to an absorption path length of 326.8 m. The FTIR spectrometer, a NICOLET Magna 550 equipped with a liquid N_2 cooled MCT detector, was operated at 1 cm^{-1} spectral resolution, and 280 to 550 scans were co-added per spectrum giving a time resolution of 5 to 15 min.

Photolysis frequencies of NO_2 were measured by 2 filter radiometers, each of which covered a 180° field of view. One of the radiometers was pointed upwards to measure the UV-flux from incoming light, the other one was pointed towards the floor to measure the flux reflected by the floor panels. Maximum daytime values for the sum of both channels are ca. $9 \times 10^{-3} \text{ s}^{-1}$.

The additional equipment used during the experiments included a gas chromatograph with flame ionisation detection (GC-FID; Hewlett Packard 6890, column: HP-5, crosslinked 5% PHME silicone 30 m \times 0.32 mm \times 0.25 μm , temperature: $T = 313 \text{ K}$, sampling rate: 4 min), a gas phase chemiluminescence NO_x -analyser with photolytic NO_2 -converter (ECO Physics CLD 770), an ozone monitor (Monitor Labs ML9810), a particle counter (TSI 3022A) and a hygrometer (Walz TS-2).

2.2 NIES

The NIES chamber has a volume of 6.065 m^3 and is a Teflon-coated (PFA-M, tetrafluoroethylene-perfluoroalkyl vinyl ether copolymer) steel cylinder with a length of 3500 mm and an inner diameter of 1450 mm. It has 20 m^2 of Teflon coated surface and 2 m^2 of glass and quartz surface, resulting in a S/V ratio of 3.7 m^{-1} . The light source is a solar simulator consisting of 19 xenon arc lamps of 1 kW each, which were operated at 800 W. The lamps are equipped with 2 mm Pyrex glass filters that cut off light of wavelengths $< 290 \text{ nm}$ to simulate tropospheric solar light. The light intensity in the chamber corresponds to an NO_2 photolysis frequency of $J(\text{NO}_2) = 4.25 \times 10^{-3} \text{ s}^{-1}$. A more detailed description of the chamber itself is given in the literature.¹⁹ Analysis of reactants and products was performed by FTIR spectroscopy, the spectrometer is a Nicolet Nexus 670 equipped with a liquid N_2 cooled MCT detector, the resolution was 1 cm^{-1} . The spectrometer is coupled to a White mirror system (base path 1700 mm) which

was operated at 130 traverses, giving to a total absorption path length of 221.5 m including the transfer path.

For the EUPHORE experiments with initial benzene concentration exceeding $1.35 \times 10^{13} \text{ cm}^{-3}$, benzene was measured by FTIR rather than DOAS due to apparent saturation effects of the UV-absorption signal for this compound. For most of these experiments, the decay of benzene was additionally monitored by GC-FID and the relative data was subsequently cross-calibrated using the initial concentration of benzene as determined with FTIR.

In this paper we use the unit “ppb” (1 ppb corresponds to $2.46 \times 10^{10} \text{ cm}^{-3}$ at $T = 298 \text{ K}$ and $p = 760 \text{ Torr}$, 1 ppm = 10^3 ppb) for mixing ratios of species as measured by NO_x - and ozone monitors or GC data and “ cm^{-3} ” for concentrations of species as measured by the spectroscopic techniques as these units correspond to the actually observed quantities.

2.3 Experimental conditions

Initial conditions of the EUPHORE and NIES experiments are given in Table 1. The initial concentration of benzene was varied between ca. $1.1 \times 10^{12} \text{ cm}^{-3}$ and $4.5 \times 10^{14} \text{ cm}^{-3}$ and that of nitrogen oxides ($\text{NO} + \text{NO}_2 = \text{NO}_x$) was varied between < 0.2 ppb and 2.0 ppm, *i.e.* over four orders of magnitude. In addition an OH-radical tracer substance (di-*n*-butyl ether, 1,3,5-trimethylbenzene or *p*-cresol) was added at concentrations of about $5 \times 10^{12} \text{ cm}^{-3}$, $7.5 \times 10^{12} \text{ cm}^{-3}$ and $6.2 \times 10^{11} \text{ cm}^{-3}$, respectively, in selected experiments in order to calculate the benzene conversion from the traced OH-profile.

Experiments were performed in very different chemical systems that use different types of OH-radical sources (see Table 1):

(1) “Photosmog” system: in this system benzene, NO and if applicable an OH-tracer were introduced into the chamber. After leaving the system approximately 30 min for stabilisation in the dark the chamber housing was opened allowing natural sunlight to start the OH-radical initiated oxidation. DOAS was operated using grating 1.

(2) Ozone-photolysis system: in this “ NO_x free” system about 60 ppb to 100 ppb of ozone in the presence of water vapour (approx. 50% relative humidity) were introduced into the chamber. The photolysis of ozone initiates the formation of OH-radicals. DOAS was operated using grating 1. After exposing the chamber to sunlight, small amounts of NO_x were observed to build up. Typical NO_x concentrations were below 2 ppb.

(3) HONO-system: about 20 ppb to 100 ppb of HONO containing NO and NO_2 were introduced into the chamber. OH-radicals were then generated from the photolysis of HONO. DOAS was operated using grating 2.

(4) H_2O_2 -system: about 5 ml of an aqueous solution of H_2O_2 (30%) were added. OH-radicals then were generated from the photolysis of H_2O_2 after opening the chamber housing. DOAS was operated using grating 1.

(5) HCHO-system: about 60 ppb of HCHO and 21 ppb of NO were added. HCHO photolysis was used to generate HO_2 radicals which were converted to OH-radicals through reaction with NO. DOAS was operated using grating 1.

(6) CH_3ONO -system: about 1 ppm of CH_3ONO and about 1 ppm of NO were added. CH_3ONO photolysis was used to generate HO_2 radicals which were converted to OH-radicals through reaction with NO.

At EUPHORE, liquid reactants were transferred to the reaction chamber from calibrated syringes by passing a stream of purified air into the chamber either through an impinger in which the desired amount was vaporised by gentle heating or through a dispersing spraying unit. *p*-Cresol was dissolved in water and sprayed into the chamber. Gaseous reactants were introduced by injecting the samples into the impinger through

Table 1 Initial conditions and results for the experiments performed at EUPHORE (BEN1 to BE31) and at NIES (NBE1 to NB43). The experimental type refers to (1) “photosmog” system, (2) ozone-photolysis system, (3) HONO system, (4) H₂O₂ system, (5) HCHO system (see text for details). The reported yields were determined by method (a) steady state assumption, (b₁) and (b₂) two kinetic approaches and (c) numerical simulation of the experimental data (see text for details)

Name	Benzene /10 ¹² cm ⁻³	NO _x (ppb)	Phenol yield, Φ _{phenol} (%)	Error of evaluation only (%)	Overall error (%)	NO _x corr.	Experimental type	Evaluation method
BEN1	58.3	95	48.0	5.5	6.9	1.03	(1)	(c)
BEN2	28.9	105	49.9	9.1	10.1	1.04	(1)	(c)
BEN3	29.3	150	44.4	11.0	11.5	1.06	(1)	(c)
BEN4	29.2	105	48.8	6.2	7.4	1.04	(1)	(c)
BEN5 ^b	57.3	195	47.7	2.5	5.2	1.09	(1)	(c)
BEN6 ^b	28.0	245	52.1	1.8	4.4	1.10	(1)	(c)
BEN7	28.3	210	47.4	4.4	6.0	1.08	(1)	(c)
BEN8 ^b	28.5	51	49.6	1.7	4.1	1.02	(1)	(c)
BEN9 ^b	11.8	100	55.3	2.8	5.7	1.04	(1)	(c)
BE10	24.1	53	55.7	6.3	7.9	1.02	(1)	(c)
BE11	1.5	50	56.1	6.0	7.4	1.02	(1)	(a)
BE12	9.9	(2) ^a	55.8	2.3	5.6	1.00	(2)	(a)
BE13	1.6	(6) ^a	58.4	6.1	7.4	1.00	(2)	(a)
BE14	1.4	(2) ^a	66.6	6.3	8.4	1.00	(4)	(a)
BE15	23.6	21	55.0	5.9	7.4	1.00	(5)	(c)
BE16 ^b	84.2	200	48.3	2.2	4.8	1.08	(1)	(c)
BE17 ^b	113.0	260	43.9	2.0	4.4	1.10	(1)	(c)
BE16II	22.1	13	57.6	7.6	9.2	1.00	(5)	(b ₂)
BE17II	13.5	135	54.5	3.2	4.5	1.04	(3)	(a)
BE18	26.8	120	50.5	8.0	9.0	1.07	(3)	(b ₁)
BE19	1.1	86	57.8	7.0	8.5	1.04	(3)	(a)
BE24 ^c	105.9	176	50.4	5.6	7.9	1.10	(3)	(b ₁)
BE26 ^c	48.9	113	50.3	2.1	5.8	1.07	(3)	(b ₁)
BE28 ^d	441.8	790	42.1	2.1	5.2	1.35	(3)	(b ₁)
BE28II ^d	411.5	1705	26.6	3.0	4.4	1.78	(3)	(b ₁)
BE31 ^{d,e}	378.2	240	53.5	4	7	1.07	(3)	(b ₁)
NBE1 ^b	122.3	1072	33.5	5.0	5.4	1.47	(1)	(b ₂)
NBE2 ^b	122.5	1084	34.6	2.2	2.9	1.46	(1)	(b ₂)
NBE3	49.7	1940	25.0	4.6	4.9	1.88	(6)	(b ₂)
NBE4	123.2	2009	25.8	1.4	2.1	2.01	(6)	(b ₂)
NB19 ^b	185.7	213	42.7	3.5	4.3	1.10	(1)	(b ₂)
NB20 ^b	183.3	106	44.8	4.3	5.1	1.05	(1)	(b ₂)
NB21 ^b	185.8	314	43.1	5.7	6.4	1.14	(1)	(b ₂)
NB43	247	121	42.1	4.9	6.8	1.06	(1)	(b ₂)

^a NO_x free at start of experiment. ^b Di-n-butylether added as tracer for OH-radicals. ^c 1,3,5-Trimethylbenzene added as tracer for OH-radicals. ^d *p*-Cresol added as tracer for OH-radicals. ^e The mixing ratio of oxygen in this experiment was raised to 40%.

a septum using syringes. In some experiments nitrous acid (HONO) was used as a source of OH-radicals. HONO was generated from an aqueous solution of NaNO₂ (1 g in 100 ml of water) dissolved in sulfuric acid (30%_{aq}). Mixtures of HONO, NO and NO₂ (approx. molar ratios of 1 : 0.9 : 0.8 respectively) were released into the gaseous phase and flushed into the chamber by an air stream. In one experiment, the mixing ratio of oxygen was raised to about 40% by flushing the reactor volume with oxygen (purity 4.5) prior to introducing the reactants.

Dilution of the reactants and products occurred by losses through small cracks in the foil and the gas flow necessary to keep the chamber inflated. To determine this dilution *ca.* 6 × 10¹¹ cm⁻³ of SF₆, an inert tracer substance, was added in all experiments. The decay of this compound was followed by FTIR spectroscopy. The leakage rate of the system (*k*_{leakage}) was typically about 5.5 × 10⁻⁶ s⁻¹.

At NIES, reactants were introduced into the chamber by vaporising the desired amount in external bulbs of known volume and flushing it into the chamber with 99.999% pure N₂. Methyl nitrite (CH₃ONO) was prepared as described previously.²⁰ The NaOH trap and N₂ stream were omitted, and the product was purified by repeated low-temperature distillations in vacuum.

2.4 Evaluation of the DOAS and FTIR spectra

All DOAS spectra were corrected for stray light, dark current and electronic offset and subsequently divided by a reference spectrum recorded the same day while the reactor was being flushed with clean air. In this way, the absorption structures of molecular oxygen, interfering with the aromatic absorption signal at wavelengths below 290 nm were virtually eliminated.²¹ The evaluation of phenol, benzene, ozone and the aromatic OH-tracer substance (if applicable) was conducted in the wavelength interval between 255 nm and 282 nm. The spectra were high-pass filtered by dividing the original spectrum by a 500 times triangular smoothed copy of itself. A new reference spectrum of benzene was recorded for each experiment at the time when only benzene was added to the chamber. For phenol and the aromatic OH-tracer substances, a spectrum was pre-recorded using the same experimental set-up. For ozone, the data of Bass and Paur²² were adjusted to match the spectral resolution of the experimental set-up. The evaluation of HONO, NO₂ and HCHO from spectra which were recorded using grating 2 was conducted in the wavelength interval between 271 nm and 363 nm using a 5th order polynomial as high-pass filter. All the fitted spectra were simultaneously adjusted using non-linear least square fitting routines of the

Mfc software.²³ A detailed description of the evaluation procedure for DOAS spectra can be found elsewhere.^{21,24,25}

The FTIR spectra were evaluated by computer-aided subtraction of calibrated reference spectra. In the evaluation of the EUPHORE data, reference spectra of phenol, formic acid, di-ⁿbutyl ether and ⁿbutyl acetate were simultaneously fitted in the region from 1075–1210 cm⁻¹, followed by nitric acid and maleic anhydride in the region 850–920 cm⁻¹. Then benzene and ozone absorptions were subtracted at 1005–1075 cm⁻¹. Due to the strong interference between the absorptions of ozone and benzene, ozone reference spectra were recorded at different temperatures and appropriate spectra were used in the subtractions. The FTIR spectrum of benzene also showed a temperature dependence that interfered with the evaluation. Therefore, the temperature dependence of the absorption cross section at 1038 cm⁻¹, which was used for the evaluations, was determined in independent experiments in a small heatable cell. The observed temperature dependence can be described by the equation

$$\sigma(T) = \sigma(T_0) - (1.77 \pm 0.05) \times 10^{-22} \text{cm}^2 \text{K}^{-1} \times (T - T_0)$$

All benzene concentrations given in this work have been corrected accordingly. Finally absorptions due to glyoxal, formaldehyde and propanal were subtracted in the region 2860–2650 cm⁻¹. Reference spectra of di-ⁿbutyl ether and its oxidation products ⁿbutyl acetate and propanal were subtracted only in those experiments where di-ⁿbutyl ether was used as an OH tracer compound. After the absorption features of all identified compounds were subtracted, the SF₆ absorption band around 947 cm⁻¹ was integrated to determine the leak rate of the chamber. The spectral subtractions of the EUPHORE data were performed using the OPUS software (version 3.0) of Bruker Messtechnik GmbH.

The NIES spectra were evaluated using the ONMIC software (version 5.1, Nicolet Inc.). Calibrated reference spectra of water (1580–1550 cm⁻¹), HNO₃ (930–840 cm⁻¹), methyl nitrite (1020–950 cm⁻¹) where applicable, formaldehyde (2830–2720 cm⁻¹), phenol (1183–1170 cm⁻¹), di-ⁿbutyl ether (1180–1100 cm⁻¹), NO (1925–1845 cm⁻¹), benzene (2030–1880 cm⁻¹), HONO (1310–1210 cm⁻¹), NO₂ (1700–1500 cm⁻¹) and O₃ (1120–950 cm⁻¹) were successively subtracted from all sample spectra. Since the NIES experiments were performed in a temperature controlled reaction chamber and the benzene absorption band evaluated was not a Q-branch, no corrections of the data for temperature dependencies were required.

Only the data of relevance to this study will be presented here. Calibrations of the DOAS and the FTIR reference spectra of aromatic compounds were performed using the cross-sections of Etzkorn *et al.*²⁶ As a cross-check, the DOAS absorption cross section of phenol was re-determined using the EUPHORE set-up. In order to compare our value of σ with the data from Etzkorn *et al.*²⁶ their spectra were adjusted to match the spectral resolution of this study. The differential absorption cross section σ' was derived from σ by a 1000 times triangular smoothing high-pass filter. The ratio of σ' divided by σ is 0.83 under the employed conditions for phenol. For the comparison the two spectra were fitted over the spectral range from 255 nm to 282 nm, *i.e.* covering three prominent differential absorption bands. Further, the FTIR cross sections of benzene and phenol were re-determined at NIES. In all cases the literature values²⁶ were confirmed within their stated error limits.

2.5 Data reduction procedures

As rate constants for the reactions of OH with benzene and phenol the temperature dependent data recommended by Atkinson⁶ were used. The values corresponding to $T = 298$ K are: $k_{\text{OH}}(\text{benzene}) = 1.23 \times 10^{-12} \text{cm}^3 \text{s}^{-1}$ and

$k_{\text{OH}}(\text{phenol}) = 2.63 \times 10^{-11} \text{cm}^3 \text{s}^{-1}$. For the OH-tracers the following rate constant values were applied: $k_{\text{OH}}(\text{di-}^n\text{butyl ether}) = 2.81 \times 10^{-11} \text{cm}^3 \text{s}^{-1}$,^{27–32} $k_{\text{OH}}(1,3,5\text{-trimethylbenzene}) = 5.73 \times 10^{-11} \text{cm}^3 \text{s}^{-1}$,^{6,32} and $k_{\text{OH}}(p\text{-cresol}) = 4.7 \times 10^{-11} \text{cm}^3 \text{s}^{-1}$.⁶ These OH reaction rate constants represent averages of the reported literature values or correspond to presently recommended values. The following four evaluation procedures (a, b₁, b₂, and c—indicated in Table 1) were employed to determine the phenol yields Φ_{phenol} :

(a) The steady-state assumption. Φ_{phenol} was determined from the measured concentrations of phenol and benzene when steady state was reached in the course of the experiments according to:

$$\Phi_{\text{phenol}} = \frac{k_{\text{OH}}(\text{phenol}) \times [\text{phenol}] \times f_c}{k_{\text{OH}}(\text{benzene}) \times [\text{benzene}]} \quad (1)$$

The correction factor $f_c = 1 + k_{\text{wall}}/(k_{\text{phenol+OH}} \times [\text{OH}])$ accounts for phenol loss to the wall. The wall deposition rate k_{wall} was determined in separate experiments yielding $k_{\text{wall}} = (7.2 \pm 3.8) \times 10^{-6} \text{s}^{-1}$ and $(1.1 \pm 0.1) \times 10^{-5} \text{s}^{-1}$ at EUPHORE and NIES, respectively. The concentration of OH was determined as described below. These corrections lead to small deviations to data presented previously.^{33,34}

(b) Direct kinetic analysis of the phenol yield. Two different approaches were applied: approach (b₁) determines the phenol yield within the first few minutes of an experiment with the advantage that loss processes of the phenol as well as effects of temperature changes are small in this phase. Approach (b₂) determines the phenol yield over a time span that is considerably longer and corrections for phenol loss through OH-reaction and wall deposition were applied and temperature changes were also considered.

(b₁) Determination of Φ_{phenol} from the phenol production rate. Eqn. (2) was used to calculate the phenol yield Φ_{phenol} from the measured production rate of phenol:

$$\Phi_{\text{phenol}} = \frac{P_{\text{phenol}}}{k_{\text{OH}}(\text{benzene}) \times [\text{OH}] \times [\text{benzene}]} \quad (2)$$

P_{phenol} denotes the average production rate of phenol over the first few minutes of reaction time as measured by the DOAS. For the time interval $t_n - t_{n-1}$, identical to the integration time of the DOAS spectra, the average OH-concentration $[\text{OH}]_{(t_n - t_{n-1})}$ was determined from the relative loss of the respective OH tracer using eqn. (3):

$$[\text{OH}]_{t_n - t_{n-1}} = \frac{\ln\left(\frac{[\text{tracer}]_{t_{n-1}}}{[\text{tracer}]_{t_n}}\right) - ((k_{\text{leakage}} + k_{\text{wall}}) \times (t_n - t_{n-1}))}{k_{\text{OH}}(\text{tracer}) \times (t_n - t_{n-1})} \quad (3)$$

The loss rates to the wall (k_{wall}) for 1,3,5-trimethylbenzene and *p*-cresol were determined to be $(3.1 \pm 2.6) \times 10^{-6} \text{s}^{-1}$ and $(1.5 \pm 0.9) \times 10^{-5} \text{s}^{-1}$, respectively, from separate experiments in EUPHORE. The wall loss of di-*n*-butyl ether, the only tracer applied at NIES and benzene was found to be negligible in both chambers. During the first few minutes of most experiments the benzene conversion was small, *i.e.* < 3% and consequently the average concentration of benzene as calculated from the OH concentration was applied in eqn. (2).

(b₂) Determination of Φ_{phenol} from the reactant–product–time series. The phenol concentrations determined experimentally were corrected for losses through reaction with OH radicals as well as wall deposition and leakage (treated as 1st order loss processes here). Eqn. (4) was used to calculate the amount

of phenol lost through both processes in the time interval t_{n-1} and t_n (see b_1):

$$[\text{phenol}]_{\text{loss}} = [\text{phenol}]_{n-1} (1 - \exp(-(k_{\text{OH}}(\text{phenol})[\text{OH}]_{(t_n-t_{n-1})} + k_{\text{wall+leak}})(t_n - t_{n-1}))) \quad (4)$$

The OH concentration $[\text{OH}]_{(t_n-t_{n-1})}$ was calculated from eqn. (3). The total amount of phenol lost from the start time t_0 of an experiment until the time t_n can then be calculated by eqn. (5):

$$[\text{phenol}]_{\text{until } t_n}^{\text{total loss}} = \sum_{i=1}^n ([\text{phenol}]_{i-1 \rightarrow i}^{\text{loss}}) \quad (5)$$

The value determined in this way was added to the experimentally observed phenol concentration at time t_n . The amount of reacted benzene was calculated from the OH-concentration $[\text{OH}]_{(t_n-t_{n-1})}$. The phenol yield was hence calculated from the slope of the corrected phenol concentration plotted as a function of the amount of reacted benzene.

After several hours of reaction time the corrected phenol concentrations were up to a factor 2 higher than the uncorrected values. Data points in which larger corrections had to be applied were discarded.

(c) Numerical simulation of reactant–product–time profiles. Phenol yields were determined by a method similar to that used for toluene experiments reported by Klotz *et al.*¹⁸ Briefly, numerical simulations were carried out in which the OH concentrations were fitted to the observed degradation rate of benzene or di-*n*-butyl ether, and yields were fitted so that the observed concentration–time profile of phenol was reproduced. The fits were performed with the FACSIMILE software package. Additional loss processes that were taken into account were reaction of phenol with OH radicals, losses through dilution of the chamber air and wall deposition.

2.6 Error considerations

The experimental error of Φ_{phenol} from individual experiments ranged between 8% and 26%. Systematic uncertainties can be broken down into the uncertainties in the absorption cross sections²⁶ (benzene: $\Delta\sigma = 2.6\%$; phenol: $\Delta\sigma = 3.9\%$) and OH-reaction rate constants (benzene:⁶ $\Delta k_{\text{OH}} = 4\%$; phenol:^{6,35} $\Delta k_{\text{OH}} \leq 6\%$; di-*n*-butyl ether:^{27–32} $\Delta k_{\text{OH}} = 3\%$; 1,3,5-trimethylbenzene:^{6,32} $\Delta k_{\text{OH}} = 9\%$; *p*-cresol:^{6,35} $\Delta k_{\text{OH}} = 11\%$) which add up to a total systematic uncertainty of Φ_{phenol} between 7.5% and 12%.

Additional error sources are due to the evaluation of the spectra (ranging from 1% to 10% (DOAS) and 2.5% to 25% (FTIR); largely determined by the signal to noise ratio of the spectra) which in most cases limited the precision with which the benzene degradation could be determined (8–25% without

added OH-tracer, 3–11% with tracer). Further minor uncertainties are due to the error of leak and wall deposition rates (0.2–4%) and changes in the reaction rate constants due to temperature changes over the course of an experiment (0.2–3%).^{30,36} Further, for the runs using radical source (2), traces of NO₂ were observed that may form NO₃ radicals from the reaction with ozone. Under the experimental conditions (ozone: 80 ppb, NO₂: 2 ppb) the NO₃ concentration may have reached levels of about 0.1 ppt corresponding to a phenol loss rate of about $9 \times 10^{-6} \text{ s}^{-1}$. This loss process may become comparable to the wall-deposition rate of phenol and was included into the errors given in Table 1 (about 3%). The overall evaluation error can be summarized for the employed evaluation methods: (a) 4% to 12%, (b₁) $\approx 2.5\%$, (b₂) $\approx 4.5\%$ and (c) $\approx 6\%$ to 25%.

The maximum error of 25% for Φ_{phenol} from the FTIR evaluation was calculated for conditions of low light intensity and the absence of a tracer substance for OH radicals. For experiments with OH tracer the overall uncertainty of Φ_{phenol} , identified as the sum of the average specific error (7.5%) and the average systematic error (10%), was 12.5%.

3. Results

A total of 26 experiments on the photo-oxidation of benzene were conducted in EUPHORE, in addition, 8 experiments were conducted at NIES. In these experiments the initial benzene concentration was varied by about a factor of 400, while the initial NO_x concentrations were varied by almost four orders of magnitude (see Table 1). The experiments presented here focus on the low-NO_x regime encompassing the NO_x levels prevailing in the atmosphere.

3.1 Phenol calibration

An advantage of the spectroscopic techniques employed for the detection of phenol is that calibration solely depends on physical properties, *i.e.* the absorption cross section spectrum $\sigma(\lambda)$ of phenol, that are independent of the measurement instrument. The UV-absorption cross section $\sigma(\lambda)$ of phenol was re-determined in a separate experiment by introducing known amounts of phenol up to a concentration of about $8 \times 10^{11} \text{ cm}^{-3}$ and recording spectra at a spectral resolution of 0.2 nm (FWHM). The phenol absorption was found to increase linearly with the introduced amount of phenol and no evidence for deviations from Lambert–Beer's law were observed under these conditions. The value of σ at 275 nm is $(1.97 \pm 0.08) \times 10^{-17} \text{ cm}^2$ and corresponds to the σ' listed in Table 2. The error of the cross section of phenol hereby is dominated by uncertainties of the exact volume of the reactor, which is known with an accuracy of approximately 3%. The result of the inter-comparison with the spectra of Etzkorn *et*

Table 2 The phenol absorption cross-section (σ) determined for this study is compared to literature values. The calibration of this study agrees well with several cross-sections that have been determined in the UV- and IR-spectral ranges. The relative calibration was scaled to the values of Etzkorn *et al.*²⁶

Reference	Spectral range ^a	Differential cross-section σ'^b	Relative calibration ^{c,d}
Bjergbakke <i>et al.</i> ¹⁰	UV : 275 nm, one band	$6.6 \times 10^{-18} \text{ cm}^2$	0.4 ± 0.08
Trost <i>et al.</i> ³⁷	UV: 245–283 nm, several bands	$1.88 \times 10^{-17} \text{ cm}^2$	1.13 ± 0.14
Etzkorn <i>et al.</i> ²⁶	UV: 248–287 nm, several bands	$1.66 \times 10^{-17} \text{ cm}^2$	1
Etzkorn <i>et al.</i> ²⁶	IR: 400–4000 cm^{-1} , several bands		1
Berndt <i>et al.</i> ³⁸	IR: 1000–4000 cm^{-1} , several bands		1.20 ± 0.12
Trost <i>et al.</i> ³⁷	IR: 1000–4000 cm^{-1} , several bands		1.10 ± 0.12
This study	UV: 255–286 nm, several bands	$1.64 \times 10^{-17} \text{ cm}^2$	0.99 ± 0.04

^a Respective spectral ranges under observation; UV: ultraviolet; IR: infrared. ^b UV: σ' of the 275 nm absorption band at a resolution of 0.2 nm (FWHM). ^c Normalised to the values of Etzkorn *et al.*²⁶ ^d FTIR: average value for four bands; integrated cross-sections were compared; see text.

^e The specified absolute $\sigma = 7.9 \times 10^{-18} \text{ cm}^2$ was multiplied by 0.83 for comparison to σ' .

*al.*²⁶ is also listed in Table 2 where the given values are scaled relative to their work due to the smaller error of σ' . Both values are in excellent agreement. Further included in Table 2 are available literature data together with the spectral ranges measured in the respective studies. The inter-comparison value for Trost *et al.*³⁷ was adopted from Etzkorn *et al.*²⁶. The two values compare well. The observed good agreement is especially interesting because Trost *et al.*³⁷ used a different calibration method based on the vapour pressure of phenol, in contrast to the method employed in this study and by Etzkorn *et al.*²⁶

An inter-comparison of the phenol measurements performed by the DOAS and FTIR systems is shown in Fig. 2. Different symbols represent the different experiments BEN1 to BE10, in which both systems were available. Only data points that overlap at least 50% of the measurement time are shown. The linear regression of the data yield: $c_{\text{phenol,FTIR}} = (1.0004 \pm 0.0053) \times c_{\text{phenol,DOAS}} - (5.6 \pm 2.0) \times 10^9 \text{ cm}^{-3}$. It is evident that the agreement between the DOAS and FTIR techniques is excellent. In Fig. 2, error bars have been included for some data points, and it becomes clear that the offset of $-5.6 \times 10^9 \text{ cm}^{-3}$ is lower than the uncertainties of the individual measurements ($\approx 7 \times 10^{10} \text{ cm}^{-3}$ for the FTIR). The errors also show that the phenol concentrations determined by DOAS are significantly more precise than those determined by FTIR. Therefore, in the experiments where both systems were available, the DOAS data have been employed in the evaluations.

This good correlation of both techniques demonstrates the quality of the phenol measurements in this work and reflects the fact that calibration of the UV and IR data is based on simultaneously determined UV and IR absorption cross sections.²⁶ Comparing our data to the independent calibration of Berndt *et al.*³⁸ and Berndt³⁹ gives agreement within $\pm 20\%$. The larger absorption cross section used in Berndt *et al.*³⁸ leads to an underestimation of the phenol yield. On the basis of our calibration their published value would correspond to 28% as indicated in Table 3.

Larger deviations are observed for the UV absorption cross section as given in the work of Bjergbakke *et al.*¹⁰ The authors measured the whole spectrum of phenol at $T = 300 \text{ K}$ and report a value for the absorption cross section at the 275 nm band, which is about a factor of 2.5 smaller than that of the other studies. We believe this discrepancy can be explained by the experimental conditions employed in the work of Bjergbakke *et al.*¹⁰ Based on the differential cross section of the pre-

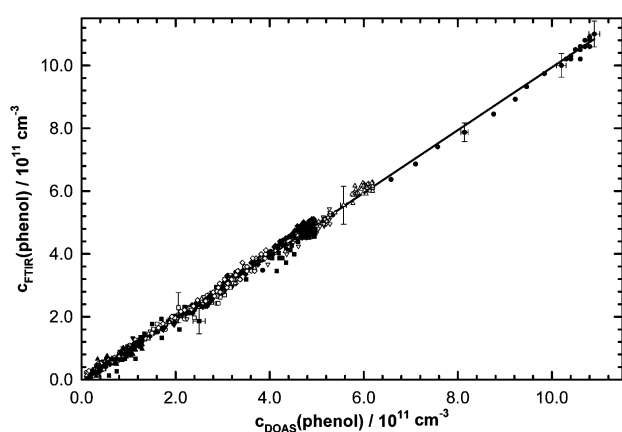


Fig. 2 Plot of phenol concentrations measured by DOAS and FTIR during experiments BEN1 to BE10 (different symbols were used for individual experiments). Only data points where the overlap of the measurement times is at least 50% have been included. Due to the significantly higher sensitivity of the DOAS instrument, the DOAS data were preferred when both systems were available.

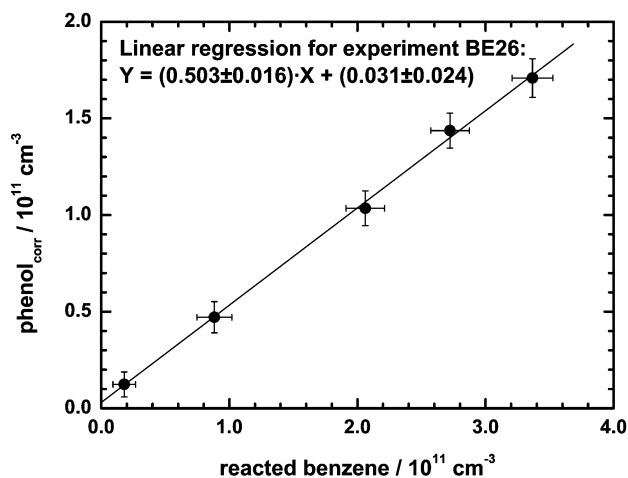


Fig. 3 Plot of the phenol produced, corrected for reaction with OH-radicals, wall loss and leakage, vs. the amount of reacted benzene as calculated from the OH-profile that was determined from the decay of 1,3,5-trimethylbenzene in experiment BE26. Phenol is identified a high yield primary product from the benzene + OH reaction in air.

sent work, the differential optical density calculated for the conditions specified by Bjergbakke *et al.*¹⁰ should have been about 2.2 (base e). If such optical densities of narrow absorption features, *i.e.* as that of phenol, are observed at a resolution that is lower than the natural line-width of the observed absorption band, deviations from Lambert–Beer’s law are likely to influence the apparent unresolved absorption signal. This was tested for benzene, comparable to phenol in this aspect, and the apparent differential absorption signal decreased by about 10% at an apparent (low resolution) optical density of roughly 0.5 (base e). Such “saturation” effects are documented in the literature^{21,40} and lead to an underestimation of the apparent absorption cross section. Given the fact that this effect is non-linear; the observed difference between the two values of a factor of 2.5 can be rationalised. If the phenol yield of 25% given by Bjergbakke *et al.*¹⁰ is based on the calibration of the present work a corrected value of 10% is obtained.

3.2 The phenol yield

The phenol yields determined for the individual experiments are listed in Table 1. In order to assess the influence of the employed evaluation procedure two errors are given (both referring to the 2-sigma confidence interval). The first error denotes the error of the evaluation procedure excluding the systematic errors due to calibration and errors in the kinetic parameters, while the second denotes the overall error of the absolute phenol yield.

In the following, three examples for the experimental data are shown. The primary phenol yield as determined during the first five minutes of experiment BE26 (see Table 1) is shown in Fig. 3. The OH profile determined from eqn. (3) was used here to calculate the amount of reacted benzene and to correct the measured phenol concentration for loss through reaction with OH (corrections $\approx 8\%$). The advantages of evaluation method b_1 (constant temperature, small corrections for secondary reactions) are here combined with the representation of the data of method b_2 . An average OH concentration of $1.3 \times 10^7 \text{ cm}^{-3}$ was determined from the decay of 1,3,5-trimethylbenzene for this experiment. The observed linear increase of phenol shows that it is a primary product in the OH initiated oxidation of benzene. The yield determined from the slope of the linear regression to the data points corresponds to a phenol yield of $(50.3 \pm 2.1)\%$.

Table 3 The phenol yield of this study in comparison with available literature values. Those studies that used spectroscopic techniques for phenol detection have been re-evaluated to match the calibration of this work (see Table 2)

Reference	Experimental setup	Conditions	Phenol yield (%)	
			Literature	Re-evaluated
Atkinson <i>et al.</i> ¹⁶	Indoor chamber, blacklamps, GC-FID	1–20 ppm NO _x in air	23.6 ± 4.4	—
Bjergbakke <i>et al.</i> ¹⁰	Ar/H ₂ O radiolysis, 275 nm absorption	NO _x free, 0–20 mbar O ₂	25 ± 5	10 ± 5
Berndt <i>et al.</i> ³⁸	H ₂ /O ₂ mw discharge, FTIR, GC-MS	NO _x free, 4–64 mbar O ₂	23 ± 7	28 ± 7
This study	outdoor and indoor chambers, DOAS/FTIR	0.002–2 ppm NO _x in air	53.1 ± 6.6	53.1 ± 6.6

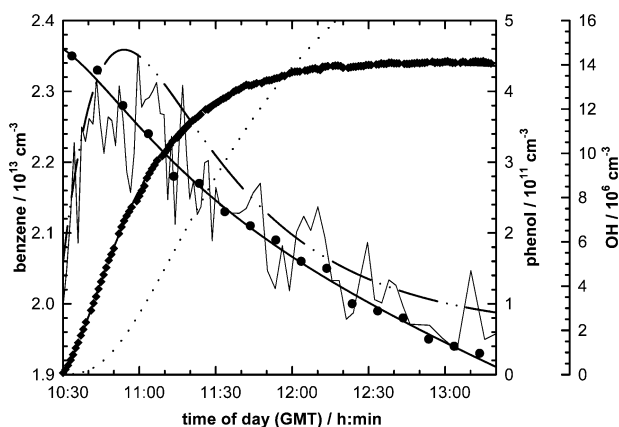


Fig. 4 Concentration–time profiles of benzene (filled circles, drawn line) and phenol (filled diamonds, dashed line) in the benzene/HCHO/NO₂ photo-oxidation experiment BE15. Also included are calculated profiles of OH radicals (dash-dot-dot line) and the amount of phenol that reacted with OH radicals (dotted line). The thin, jagged line represents OH radical concentrations experimentally determined with an LIF apparatus.

Fig. 4 shows the results of the numerical simulation of EUPHORE experiment BE15, an experiment without added OH tracer. In this experiment, some formaldehyde was added to the reaction mixture to enhance the reactivity of the system. The high radical concentrations in this experiment lead to a

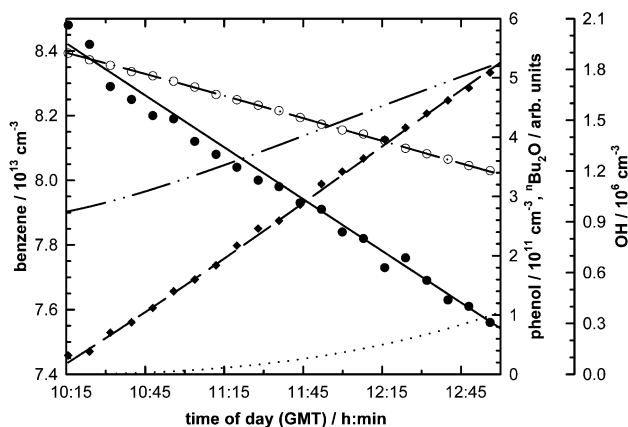


Fig. 5 Experimental (symbols) and calculated (lines) concentration–time profiles of benzene (filled circles, drawn line), di-ⁿbutyl ether (open circles, dot-and-dash line) and phenol (filled diamonds, dashed line) in the benzene/NO photo-oxidation experiment BE16. Also included are calculated profiles of OH radicals (dash-dot-dot line) and the amount of phenol that reacted with OH radicals (dotted line).

high turnover of benzene, and despite the fact that a large proportion of the phenol is reacting with OH radicals (see the dotted line in Fig. 4), the calculated concentration–time profile of phenol closely matches the measured one. The thin jagged line included in Fig. 4 shows an experimentally determined concentration–time profile of OH radicals. This profile was measured with an LIF (laser induced fluorescence) device, which had been installed in the chamber just prior to this experiment.⁴¹ The device was undergoing first tests during this experiment, and though the measured OH concentration–time profile shows a *ca.* 20% lower maximum concentration than calculated from the benzene decay, the agreement is generally satisfactory. The performance of the methods employed to calculate the OH radical concentrations from the hydrocarbon decays is hence confirmed by these direct OH measurements, though only in a single experiment.

As an example for an experiment with added OH tracer substance, the EUPHORE experiment BE16 is shown in Fig. 5. In this experiment, only about 15% of the phenol formed reacted with OH radicals, and the overlap between the calculated and measured phenol profile is again excellent. It is further apparent from Fig. 5 that even though the OH radical concentration has been fitted to the decay of di-*n*-butyl ether, the degradation of benzene is reproduced well by this procedure, further supporting the validity of the evaluation method employed here. Since further experiments where a large correction was necessary, *e.g.* BE15 (Fig. 4), resulted in the same phenol yields as those with very small corrections, *e.g.* BE16 (Fig. 5), the corrections for phenol loss are believed to be accurate.

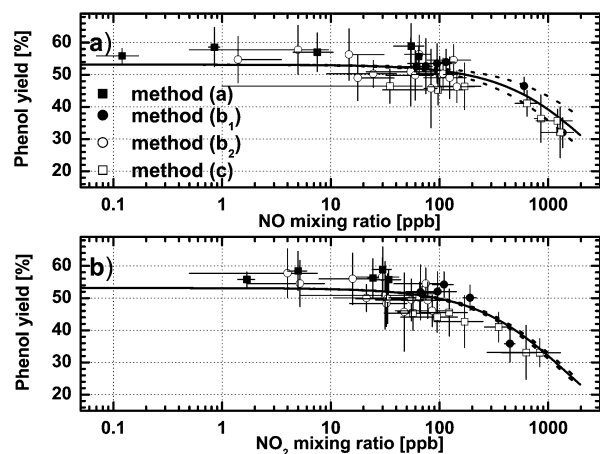


Fig. 6 The phenol yield as a function of the mixing ratio of (a) NO, corrected for the NO₂ influence and (b) NO₂, corrected for the NO influence. Different symbols represent the different evaluation methods (a) to (c) (see text). The black line is calculated from the simplified eqn. (6) (see text). The decreasing phenol yields at high mixing ratios of NO_x indicate a change in the oxidation mechanism of benzene.

3.3 Dependence of the phenol yield on the NO_x concentration

Fig. 1 shows the initial reaction steps of the oxidation of benzene. Given these loss processes from the equilibrium of intermediates **2/3** the phenol yield Φ_{phenol} is described by eqn. (6):

$$\Phi_{\text{phenol}} = \frac{k_{\text{phenol}} + \frac{\Phi_{\text{phenol},10} \times k_{10}[\text{NO}_2]}{K_{\text{eq}}[\text{O}_2]}}{k_{\text{phenol}} + k_8 + \frac{k_9}{K_{\text{eq}}} + \frac{k_{10}[\text{NO}_2]}{K_{\text{eq}}[\text{O}_2]} + k_{12}[\text{NO}]} \quad (6)$$

Whereby, the following simplifications have been made:

(i) The effective sum of the pathways that form phenol is defined as $k_{\text{phenol}} = k_3/K_{\text{eq}} + k_4$.

(ii) The dissociation reaction (–1) of **2** was not considered since it accounts for less than one percent of the total loss rate from the equilibrium **2/3** under atmospheric conditions.^{7,8}

(iii) The rate constant for channel (5) was set to zero based on the results of Bohn and Zetsch⁸ who estimate an upper limit of 5% for this pathway.

(iv) The rate constant for channel (6) was assumed to be zero.

(v) $\Phi_{\text{phenol},10}$ was set to zero in the further evaluation, reflecting the negligible contribution of channel (10) to the observed phenol under the conditions employed in this work (see below).

(vi) Channel (11) was assumed to be essentially negligible for NO concentrations under 10 ppm and hence is not considered here.⁷

The following rate coefficients were used that are valid for 298 K and atmospheric oxygen concentrations: $K_{\text{eq}} = (2.7 \pm 0.4) \times 10^{-19} \text{ cm}^3$, $k_{\text{tot}} = (k_3 + k_9)/K_{\text{eq}} + k_4 + k_8 = (760 \pm 80) \text{ s}^{-1}$, $k_{10} = (2.75 \pm 0.2) \times 10^{-11} \text{ cm}^3 \text{ s}^{-1}$, $k_{12} = (1.1 \pm 0.4) \times 10^{-11} \text{ cm}^3 \text{ s}^{-1}$.^{7,8}

The experimental data of the phenol yield as determined in the individual experiments of this study are shown in Fig. 6. The errors of the phenol yield correspond to the specific error sources of the evaluation method only. The error bars with respect to NO_x values in Fig. 6 correspond to the variability of the respective NO_x species over the time span of evaluation. In panel (a) the phenol yield is given as a function of the NO mixing ratio, in (b) it is given as a function of the NO₂ mixing ratio. The solid line indicates the theoretical phenol yield as calculated from eqn. (6), with a correction for the influence of NO₂ in the curve plotted in panel (a) and a correction for the influence of NO in panel (b). Correction factors were calculated as the ratio of equation (6) assuming $k_{10} \neq 0$ divided by eqn. (6) assuming $k_{10} = 0$ to correct for the NO₂ influence in Fig. 6a. These factors for most experiments were smaller than 1.035 with a maximum of 1.34. Accordingly, in Fig. 6b the corrections for NO were calculated assuming $k_{12} = 0$ and $k_{12} \neq 0$. Here, the factors ranged between 1.0 and 1.22. The NO and NO₂ values used in the corrections are taken from the experimental data averaged over the time period when the phenol yield was determined. The phenol yields shown in Figs. 6a and 6b correspond to the experimental data (Table 1) multiplied with the factors of the NO₂ and NO correction, respectively. The dotted lines in Fig. 6 indicate respective uncertainties in the rate constants k_{10} and k_{12} . As can be seen, the simplified eqn. (6) (*i.e.* assuming $\Phi_{\text{phenol},10} = 0$, see above) equally well describes the dependence of the phenol yield with respect to NO and NO₂. The data further indicates that the phenol yield is more sensitive on the presence of NO₂ than on NO, reflecting the fact that k_{10} is about 2.5 times faster than k_{12} . Within the uncertainties excluding systematic errors all data points are in good agreement with the calculated phenol yields indicating that the mechanism described by eqn. (6) is suitable to represent the

observed dependence of the phenol yield on the NO_x concentration under our experimental conditions.

In Table 1 the numbers listed in the column denoted “NO_x corr.” were calculated from eqn. (6) to reflect the influence of the NO_x reactions. The maximum correction factor of 2 corresponds to the case when oxygen and NO_x reactions determine the loss from equilibrium **2/3** to equal amounts. The numbers for most experiments are considerably lower indicating that under the experimental conditions of this work the overall loss from equilibrium **2/3** was dominated by reactions involving oxygen.

3.4 The average phenol yield

The parameter k_{phenol} in eqn. (6) was determined as follows. All the experiments with added OH-tracer were considered (see Table 1). In addition, BE15 was considered due to the enhanced benzene turnover and the correspondingly reduced error of this experiment, see Fig. 4. Further considered were the experiments that were evaluated from method (a) since the phenol yield in this case is essentially not influenced by uncertainties in the OH concentration. The yields of the individual experiments were corrected for NO_x influence using the correction factors listed in Table 1. Experiments with correction factors > 1.4 were neglected. Not considered were the experiments with low benzene turnover where no OH-tracer substance had been added as well as experiment BE14 due to the substantially higher phenol yields which were observed under NO_x-free conditions in the presence of H₂O₂.

Independent of the evaluation procedure the yields were found to coincide within the specific evaluation error. The average phenol yield from the experiments was (53.1 ± 6.6)%. The error hereby represents the overall 2-sigma confidence interval.

Based on the value for the total loss from the equilibrium **2/3**, *i.e.* $k_{\text{tot}} = (760 \pm 80) \text{ s}^{-1}$,⁸ the average phenol yield corresponds to a value of $k_{\text{phenol}} = (404 \pm 66) \text{ s}^{-1}$ in eqn. (6). Consequently, the value of the effective sum of loss rates through channels (8) and (9), *i.e.* $k_{\text{other products}} = (k_{\text{tot}} - k_{\text{phenol}}) = (k_9/K_{\text{eq}} + k_8)$ is estimated to $k_{\text{other products}} = (356 \pm 59) \text{ s}^{-1}$.

3.5 The oxygen dependence of the phenol yield

In a single experiment (BE31, Table 1) the mixing ratio of oxygen was raised to about 40%. No effect on the phenol yield was observed; the yield of (53.5 ± 4.0)% agrees well with the average yield determined in air. This result further confirms eqn. (6) under low NO_x conditions where the reactions (10) and (12) (Fig. 1) are unimportant and the intermediates **2/3** primarily react with oxygen.

It should be noted, however, that the phenol yield as calculated from eqn. (6) is expected to depend on the oxygen concentration under conditions where the influence of reaction (10) is non-negligible.

3.6 The temperature dependence of the phenol yield

Those phenol yields used to determine the average phenol yield are plotted as a function of temperature in Fig. 7a. The solid line denotes an error weighted linear regression to the data points. For relative comparison the plotted error bars correspond to the 2-sigma confidence interval neglecting systematic error sources, which would not influence the T-dependency. The annual cycle of the ambient temperature of EUPHORE is reflected in the temperature scale that covers about 20 K. An upper limit of about 307 K (34 °C) corresponds to a hot day during summer while the lower limit of about 287 K (14

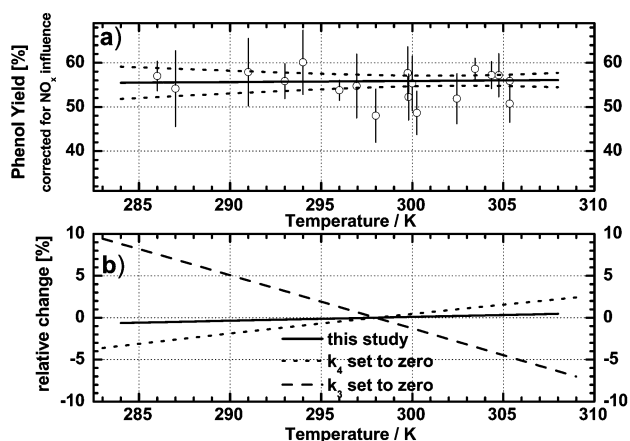


Fig. 7 The phenol yield as a function of the temperature for experiments with OH-tracer. In the upper parts the experimental data was corrected for the NO_x influence from eqn. (6), see text. In the lower part, the relative change of the phenol yield is estimated from the enthalpy data of Lay *et al.*⁹ and compared to the observed variation. The result tends to support the formation of phenol from pathway (3) in Fig. 1.

°C) reflects typical temperatures in EUPHORE during winter. The data points are described by the following expression: $\Phi_{\text{phenol}}(T) = (0.026 \pm 0.1)(T - T_0) + \Phi_{\text{phenol}}(T_0)$ (see Fig. 7a). Though the slope is positive it is essentially zero within the experimental error.

Attempts were made to use the enthalpy data from the study of Lay *et al.*⁹ to estimate whether channel (3) or channel (4) leads to the formation of phenol. The enthalpy and entropy data of Lay *et al.*⁹ is in reasonable agreement with the measured K_{eq} value of Bohn and Zetsch.⁸ From this data, K_{eq} is expected to change by a factor of five over a 20 K temperature range around room temperature. Further, Lay *et al.*⁹ give detailed enthalpy data for the rate constants k_3 , k_4 , k_8 and k_9 that essentially determine the phenol yield here. Even though the calculated absolute values for these rate constants may be wrong⁸ the enthalpy data provides a means for an adequate description of the variations of the rate constants with temperature. The values of k_3 , k_4 , k_8 and k_9 from Lay *et al.*⁹ were scaled linearly (by ≈ 24 for k_3 and k_4 ; by ≈ 7 for k_8 and k_9) to match the absolute value of k_{phenol} and $k_{\text{other products}}$ using K_{eq} from Bohn and Zetsch⁸ at $T = 296$ K. Eqn. (6) could then be used to calculate the temperature dependent phenol yield. In Fig. 7b the relative change of the phenol yield is shown for two scenarios. First, k_3 was set to zero (dashed line) and second, k_4 was set to zero (dotted line). In addition, the relative change of the phenol yield from the regression to the experimental data is included (solid line). The three lines are normalised to $T = 298$ K in this representation.

As can be seen in Fig. 7b, the two phenol-forming channels (3) and (4) exhibit distinctly different temperature dependencies. In the case of only channel (3) forming phenol the yield is expected to increase with temperature, though only slightly, with an assumed linear relative change of $+0.23\% \text{ K}^{-1}$. In contrast, if only channel (4) forms phenol a pronounced decrease of the phenol yield is expected at a rate of $-0.63\% \text{ K}^{-1}$. This characteristic behaviour can, in principle, be used to distinguish both channels even within the small temperature interval covered by this study. From the slope of the linear regression to the data points a relative change of $(0.05 \pm 0.2)\% \text{ K}^{-1}$ is obtained which is consistent with channel (3) contributing about $(80 \pm 25)\%$ of the phenol and channel (4) contributing about $(20 \pm 25)\%$. Despite the large errors this result points to channel (3) being the major, and possibly only route to the formation of phenol.

3.7 Primary and secondary phenol formation

Attempts were made to distinguish between the relative contributions of pathways 3 to 5 in Fig. 1 that result in the direct formation of phenol (primary phenol) and pathway 6 which forms phenol *via* the stable, *i.e.* “long-lived”, intermediate compound benzene oxide/oxepin (secondary phenol).¹³

The photolysis of benzene oxide/oxepin, reaction (7) in Fig. 1 forms phenol at a yield of $(43.2 \pm 4.5)\%$.^{13,42} Additionally, the reaction with OH-radicals is fast with a rate constant of $k_{\text{OH}}(\text{benzene oxide/oxepin}) = 1 \times 10^{-10} \text{ cm}^3 \text{ s}^{-1}$.¹³ Assuming an OH radical concentration of $3 \times 10^6 \text{ cm}^{-3}$ and an NO₂ photolysis frequency of $J(\text{NO}_2) = 8.5 \times 10^{-3} \text{ s}^{-1}$ (typical for the experiments conducted at EUPHORE) the losses of benzene oxide/oxepin due to photolysis and OH-reaction are about equal. Thus, even assuming a unity yield for the formation of benzene oxide/oxepin in the OH initiated oxidation of benzene, the reaction sequence (6/7) in Fig. 1, if occurring, could form no more than 40–50% of the observed phenol.

The overall loss rate of benzene oxide/oxepin in this example is about $6.8 \times 10^{-4} \text{ s}^{-1}$, which corresponds to a lifetime of roughly 25 min. Hence, the formation of secondary phenol *via* pathway (6/7) should become operative with considerable delay and should influence the formation kinetics of phenol during the first few minutes of reaction time to a very minor extent. Nevertheless, the primary phenol yield determined for experiment BE26 in Fig. 4, see Table 1, compares well to the yield as calculated from eqn. (6) of $(52.1 \pm 0.4)\%$ for the corresponding NO and NO₂ concentrations of BE26. Since eqn. (6) fits the phenol yields determined after several hours of reaction time equally well (*e.g.* experiment BE12, Fig. 5) there is no indication that pathway (6/7) contributes to the observed phenol formation.

Further, the numerical simulations conducted in this study adequately reproduced the concentration–time profile of phenol by a mechanism involving only channel (3), as is evident from Fig. 3 and Fig. 6. This study, therefore, provides no evidence to support that channel (6/7) is operative in the OH initiated oxidation of benzene. The combined experimental errors from the relative comparison of two phenol yields, *i.e.* at the very start (BE26) and after several hours of reaction time (BE12) is 3.1%. Under the conditions of experiments BE12 and BE26 about 26% and 34% of benzene oxide/oxepin if formed would be expected to photolyse, respectively. Hence, an upper limit for the formation of benzene oxide/oxepin of about 24% can be estimated on the basis of the uncertainty of the phenol yields.

4. Discussion

4.1 The phenol yield found in the literature

The phenol yield obtained in this study is compared to literature values in Table 3. It is evident that the value given here is about twice as high as the previously reported values. There are two previous studies^{10,38} that used spectroscopic techniques for the detection of phenol. The results of these have been scaled to match the calibrations used in this work, the corrected values are given in the column “re-evaluated values” in Table 3. As can be seen, the apparent previous good agreement between literature values shows considerable scatter if placed on a common basis of calibration.

The phenol yield reported by Bjergbakke *et al.*¹⁰ was calculated based on residual absorptions observed at a wavelength of 275 nm in a pulse radiolysis study. The OH concentration observed around 309 nm was used to calculate the benzene decay at a temperature of $T = 340$ K. A considerably lower phenol yield at this temperature would be in contradiction to the enthalpy data from Lay *et al.*⁹ and would further contradict the observed temperature dependence of this work. The

difference in the yields is too high in order to be explained on the basis of a temperature change of 40 K. The reason for the differences in the phenol yield may be found in the high radical concentrations that Bjergbakke *et al.*¹⁰ reported for their system. Given the considerably lower re-evaluated phenol yield of 10%, residual reactions that were not completely suppressed may have had significant influence. In the presence of oxygen, the high concentrations of H atoms produced in the pulse radiolysis would form HO₂ radicals which react with the aromatic-OH adduct thus introducing an additional loss process from the equilibrium 2/3 which could explain the lower phenol yield. In addition, an uncertainty about the experimental conditions arises from the proposed formation mechanism of phenol, that Bjergbakke *et al.*¹⁰ attribute to channel (5) in Fig. 1. This conclusion is in conflict with a recent study⁸ in which an upper limit of 5% is determined for this reaction.

The phenol formation yield given by Berndt *et al.*³⁸ was determined in a flow system using FTIR spectrometry for the detection of both benzene and phenol. OH radicals were generated by microwave discharge of H₂ in the presence of O₂. The resulting HO₂ radicals gave OH by self-reaction. According to the authors, no corrections of measured product concentrations for secondary reactions were necessary. However, this appears to be in contrast to the observation of CO and formic acid as products of the benzene + OH reaction, which, according to all currently proposed benzene degradation schemes, should be secondary products. Also, the two strongest absorptions observed in the residual FTIR spectra of Berndt *et al.*³⁸ (Fig. 3 in that paper) are very similar to those of *E,E*-2,4-hexadienedial published by Klotz *et al.*⁴³ The most likely pathway for the formation of this compound under NO_x free conditions is reaction of the hydroxycyclohexadienyl peroxy radical (3 in Fig. 1) with another organic peroxy radical RO₂ to give a hydroxycyclohexadienyl oxyl radical, an RO radical and O₂. The hydroxycyclohexadienyl oxyl radical can then ring-open and react with O₂ to give HO₂ and *Z,Z*-2,4-hexadienedial, which can isomerise to the more stable *E,E*-2,4-hexadienedial. If this were the case in the study of Berndt *et al.*,³⁸ it would indicate the presence of extremely high radical concentrations in their reaction system. This reaction sequence would represent an additional loss channel of hydroxycyclohexadienyl peroxy radicals 3 not present under atmospheric conditions, which could explain the lower phenol yields. Alternatively, an intramolecular H transfer from the OH group to the peroxy group of 3, followed by elimination of OH may also account for the formation of *E,E*-2,4-hexadienedial, but this channel is thought to be energetically unfavourable.⁹ Additionally, this pathway would also be operative under the conditions of the present study, however, no *E,E*-2,4-hexadienedial was observed in our experiments. An upper limit for the formation yield of hexadienedials from benzene was determined in a recent study, conducted under conditions comparable to those of this work, to be 8%.¹⁵

In summary, a definite reason for the observed discrepancy between the phenol formation yields under NO_x-free conditions determined in this study and those reported in the literature can not be given here. It may be speculated that due to different experimental conditions, different formation mechanisms are involved in the different studies.

The study of Atkinson *et al.*¹⁶ was conducted in a 6.4 m³ reaction chamber, OH radicals were generated by blacklight irradiation of CH₃ONO/NO_x/air mixtures with the initial NO_x concentration being varied between about 1 ppm and 20 ppm. Benzene was determined by GC-FID, phenol by collecting samples on Tenax adsorbent followed by GC-FID analysis. Corrections were applied for secondary reactions of phenol with OH radicals. The lower phenol yield is qualitatively in agreement with the interference of high NO_x levels expected according to eqn. (6). A direct comparison with eqn. (6) suffers from the marginal overlap of the NO_x concen-

trations employed. However, from the scatter in their plotted data (Fig. 5 of Atkinson *et al.*¹⁶) it appears that the phenol yield rather ranged between 19.4% and 34.8%. Thereby, the latter value corresponds to the lowest of their employed NO_x concentrations and is comparable to the yield calculated from eqn. (6) (experiment ITC#1295, [NO] ≈ [NO₂] ≈ 0.62 ppm: $\Phi_{\text{phenol,eq6}} = 32.4\%$). This good agreement confirms eqn. (6) to be valid up to NO_x concentrations of about 2 ppm without any major contribution of phenol from the NO_x reactions under the experimental conditions of this work (note that the loss from equilibrium 2/3 is still dominated by reactions involving oxygen here).

It is, however, noteworthy that Atkinson *et al.*¹⁶ observed no systematic dependency of the phenol yield on the NO_x concentration. This may be explained from eqn. (6) on the basis of a significant phenol yield of the reaction of the benzene-OH adduct 2 with NO₂. This reaction may become a significant source of phenol at high NO_x concentrations. At present, the value of $\Phi_{\text{phenol,10}}$ is not known. Due to the fact that the NO_x concentrations employed in this study were generally much lower than those of Atkinson and because mainly NO was present initially, it is not possible to estimate $\Phi_{\text{phenol,10}}$ on the basis of the data of this work. Further experiments under conditions of high NO_x concentrations are required in order to elucidate the presently unknown dependency of the phenol yield on the NO- and NO₂ concentrations, which is a prerequisite to understand the phenol formation under conditions of high NO_x (ppm range) as they are prevalent in many laboratory studies.

4.2 The influence of the oxygen concentration

The elevated concentration of oxygen employed in experiment BE31 was found to have no influence on the phenol yield under the comparably low NO_x concentrations employed in this work, in agreement with eqn. (6). Though the phenol yield from this experiment tends to be slightly higher than the values observed in air at comparable NO_x concentrations (see Table 1) it compares well with the average phenol yield determined in this work from the NO_x corrected values and thereby further confirms eqn. (6).

However, the present data is not sufficiently extensive to demonstrate the oxygen concentration dependence of Φ_{phenol} as it is predicted from eqn. (6) under different experimental conditions, when the influence of reaction (10) is significant. Notably, equation (6) does not predict an oxygen concentration dependence of the reaction of 3 with NO. Hence, according to eqn. (6) it should be possible to vary the relative importance of influencing NO and NO₂ reactions by varying the oxygen concentration. This would give a handle to discriminate between intermediates 2 and 3 with respect to the loss processes from equilibrium 2/3. A systematic study of the oxygen concentration dependence of the phenol yield, predicted from eqn. (6) under conditions of high NO_x, is desirable.

4.3 Additional support for the high phenol yield from recent studies

Further evidence for the high phenol yield comes from a recent comparative smog chamber study on the glyoxal yield at the EUPHORE facility under similar experimental conditions as in this work. Volkamer *et al.*¹⁵ compared the ratio of the glyoxal production rate to that of a respective ring-retaining product from benzene, toluene and *p*-xylene (BTX). In all three systems this ratio was observed to be constant. For the toluene and *p*-xylene system these ratios were found to be compatible with the well-known yields of benzaldehyde and the *p*-tolualdehyde, respectively. However, the observed ratio in the

benzene system could not be explained on the basis of low phenol yield of $\approx 25\%$. It was found to be more consistent with the high phenol yield of this study.

Finally, a high phenol yield of around 50% is also consistent with the results of a recent study by Bohn and Zetzsch⁸ who indirectly determined the formation of HO₂ radicals through channels (3) or (4) in Fig. 1. Despite the large error, Bohn and Zetzsch⁸ concluded that the observed yield of “prompt” HO₂ is higher than the 25% inferred from previous phenol yields.

4.4 Atmospheric implications

The phenol yield obtained for NO_x concentrations of several 10 ppb is essentially constant. Hence, the value of $\Phi_{\text{phenol}} = (53.1 \pm 6.6)\%$ should be representative for the boundary layer, including most conditions of the urban atmosphere. Under conditions with exceptionally high NO_x concentrations, *i.e.* near the exhaust pipe of cars or near traffic tunnels, the phenol yield from the OH initiated oxidation of benzene may be lower, but such conditions can only have a negligible effect on atmospheric phenol concentrations.

Despite the comparably low reactivity of benzene compared to the alkyl-substituted aromatics hydrocarbons, considerable amounts of phenol will be formed from the OH-initiated degradation of benzene. The expected higher amounts of phenol formed in the atmosphere will also mean that a more detailed understanding of its sinks is desirable. It is generally assumed that OH radical initiated loss is the principal fate of phenol during the day, while NO₃ reactions were recognized by Carter *et al.*⁴⁴ to be an important sink especially during the night. In recent years the estimates of the daytime NO₃ concentration have improved considerably, and despite remaining uncertainties^{45,46} range between 2.5×10^6 molec cm⁻³ and 1.2×10^7 molec cm⁻³ in semi-rural⁴⁶ and urban atmospheres,^{47,48} *i.e.* are comparable to, or even above the daytime concentration of OH radicals (about 4×10^6 molec cm⁻³).⁴⁹ For phenol the OH reaction rate constant is only about seven times faster than the corresponding value for the NO₃ reaction.⁶ Hence, the radical initiated loss of phenol, though dominated by OH reactions under most conditions, is influenced by the daytime NO₃ + phenol reaction to about 10 to 40%. The importance of daytime NO₃ reactions may even dominate over OH reactions in polluted air masses, whenever high levels of NO₂ are present and ozone levels exceed NO levels, thus promoting the formation of NO₃, while lowering the OH-level (*i.e.* via the reaction NO₂ + OH + M → HNO₃ + M). The portion of daytime NO₃ reactions will further be higher for the phenol-type products of alkylbenzenes (*i.e.* toluene, xylenes *etc.*).⁵⁰ During the night, when NO₃ levels are generally much higher (exceeding OH levels by three to four orders of magnitude), the NO₃ reaction will be the predominant sink of phenol. Notably, few studies exist on the NO₃ reaction of phenol and, in addition, its potential loss to the liquid phase (*i.e.* Henry constants) is ill understood at present.

Another interesting aspect of the high phenol yield is that ring-retaining pathways account for 53% of the overall degradation routes of benzene. These are assumed to be not as effective as the ring-cleavage pathways with respect to the formation of photo-oxidants.⁵¹ The high phenol yield implies a reduced photo-oxidant formation from benzene as compared to the alkylated aromatics from which lower yields of ring-retaining pathways are observed.^{18,33,34,16,52,53}

The observed decrease of the phenol yield with increasing NO_x concentration indicates a change in the oxidation mechanism of benzene. At high NO_x concentrations, reactions (10) and (12) (Fig. 1) become competitive to reactions (3) to (9), opening reaction pathways that most likely lead to a product distribution different to that obtained *via* reactions (3) to

(9). Nevertheless, both reactions (10) and (12) are expected to be essentially unimportant in most parts of the atmosphere.

5. Conclusions

This study represents the first determination of phenol yields in the OH initiated oxidation of benzene under truly atmospheric conditions. The concentrations of both benzene and NO_x could be lowered to levels found in the polluted urban atmosphere. The phenol yield was found to be $(53.1 \pm 6.6)\%$, about twice as high as previous studies. With respect to the formation mechanism of phenol our data is in line with a direct phenol formation proceeding from the reaction: benzene + OH + O₂ → phenol + HO₂. Thereby, about $(80 \pm 25)\%$ of the direct phenol formation proceeds from the reaction of the benzene-OH adduct with oxygen. There is no evidence for the involvement of benzene oxide/oxepin in phenol formation, an upper limit of 24% is estimated for the formation yield of this compound in the OH initiated oxidation of benzene.

The high phenol yield of this work is found to be essentially independent of the NO_x concentrations under the conditions prevalent in the urban atmosphere. At elevated NO_x concentrations (> 100 ppb), which are typical for previous smog chamber studies, the phenol yield is observed to decrease. This NO_x dependence of the phenol yield is adequately described by eqn. (6) and indicates a change in the oxidation mechanism of benzene. Under our experimental conditions the NO_x reactions (channels (10) to (12) in Fig. 1) do not appear to contribute significantly to the observed phenol.

With respect to future work on the benzene system a temperature and oxygen concentration dependent study of the phenol yield over a wider range of experimental conditions is desirable. As an outcome of the re-evaluation of the phenol yields from literature studies conducted under NO_x free conditions considerable scatter became evident among the previously apparent good agreement between these values. A definitive explanation of the differences can not yet be given and additional research is needed to elucidate the phenol formation under NO_x free conditions. Similarly, the phenol forming chemistry under elevated concentrations of NO_x (several ppm) remains unclear and will be the subject of a forthcoming paper. This is of particular importance because most chemical mechanisms used for photo-oxidant modelling are validated against high-NO_x smog-chamber data, and may therefore not be representative of the troposphere.

Acknowledgement

Financial support of this work by the “Bundesministerium für Bildung, Wissenschaft, Forschung und Technologie” (BMBF) within grant 07TFS30 is gratefully acknowledged. R. V. acknowledges a Marie Curie fellowship from the European Commission DG-XII, Environment and Climate Programme under contract No. ERB 4001GT970196. Further, Jens Uecker, Klaus Brockmann, Manfred Siese and Milagros Ródenas are acknowledged for their support in the experiments. B. K. is grateful to the Japanese Science and Technology Agency (STA) and the Alexander von Humboldt Foundation for a fellowship. The CEAM Foundation is supported by the Generalitat Valenciana and BANCAIXA.

References

- 1 S. D. Piccot, J. J. Watson and J. W. Jones, *J. Geophys. Res.*, 1992, **97**, 9897.
- 2 S. Legett, *Atmos. Environ.*, 1996, **30**, 215.

- 3 J. G. Calvert, R. Atkinson, K. H. Becker, R. M. Kamens, J. H. Seinfeld, T. J. Wallington, G. Yarwood, *The Mechanisms of Atmospheric Oxidation of Aromatic Hydrocarbons*, Oxford University Press, 2002.
- 4 Directive 2000/69/EC of the European Parliament and of the Council of 16 November 2000 relating to limit values for benzene and carbon monoxide in ambient air, *Official Journal of the European Union*, 2000, **L313**, 12.
- 5 J. J. Bufalini, *Identification of Hazardous Products formed During Photochemical Transformation of Pollutants*, NSI P.O. No. 8806RG1852, BATELLE Final Report, 1989.
- 6 R. Atkinson, *J. Phys. Chem. Ref. Data*, 1994, **Monograph No. 2**, 1.
- 7 R. Knispel, R. Koch, M. Siese and C. Zetzsch, *Ber. Bunsen-Ges. Phys. Chem.*, 1990, **94**, 1375.
- 8 B. Bohn and C. Zetzsch, *Phys. Chem. Chem. Phys.*, **1**, 5097.
- 9 T. Lay, J. Bozzelli and J. H. Seinfeld, *J. Phys. Chem.*, 1996, **100**, 6543.
- 10 E. Bjergbakke, A. Sillesen and P. Pagsberg, *J. Phys. Chem.*, 1996, **100**, 5729.
- 11 R. Koch, *J. Phys. Chem. B*, 1997, **101**, 293.
- 12 P. Pagsberg, *J. Phys. Chem. B*, 1997, **101**, 294.
- 13 B. Klotz, I. Barnes, K. H. Becker and B. T. Golding, *J. Chem. Soc., Faraday Trans.*, **93**, 1507.
- 14 J. Yu, and H. Jeffries, *Atmos. Environ.*, 1997, **31**, 2281.
- 15 R. Volkamer, U. Platt and K. Wirtz, *J. Phys. Chem. A*, 2001, **105**, 7865.
- 16 R. Atkinson, S. M. Aschmann, J. Arey and W. P. L. Carter, *Int. J. Chem. Kinet.*, 1989, **21**, 801.
- 17 EUPHORE, ed. K. H. Becker, Final Report to the European Commission, Contract #EV5V-CT92-0059, Bergische Universität Wuppertal, Germany, 1996.
- 18 B. Klotz, S. Sørensen, I. Barnes, K. H. Becker, T. Etkorn, R. Volkamer, U. Platt, K. Wirtz and M. Martín-Reviejo, *J. Phys. Chem. A*, 1998, **102**, 10289.
- 19 H. Akimoto, M. Hoshino, G. Inoue, F. Sakamaki, N. Washida and M. Okuda, *Environ. Sci. Technol.*, 1979, **13**, 471.
- 20 W. D. Taylor, T. D. Allston, M. J. Moscato, G. B. Fazekas, R. Kozlowski and G. A. Takacs, *Int. J. Chem. Kinet.*, 1980, **12**, 231.
- 21 R. Volkamer, T. Etkorn, A. Geyer and U. Platt, *Atmos. Environ.*, 1998, **32**, 3731.
- 22 A. Bass and R. Paur, *Proc. Quadrenn. Ozone Symp.*, Chalkidiki, Greece, 1985, p. 606.
- 23 T. Gomer, T. Brauers, F. Heintz, J. Stutz and U. Platt, MFC User Manual, Vers. 1.98, Universität Heidelberg, 1993.
- 24 U. Platt, in *Air Monitoring by Spectroscopic Techniques*, ed. M. W. Sigrist, John Wiley & Sons, 1994, p. 27.
- 25 J. Stutz and U. Platt, *Appl. Opt.*, 1996, **35**, 6041.
- 26 T. Etkorn, B. Klotz, S. Sørensen, I. V. Patroescu, I. Barnes, K. H. Becker and U. Platt, *Atmos. Environ.*, 1999, **33**, 525.
- 27 T. J. Wallington, R. Liu, P. Dagaut and M. J. Kurylo, *Int. J. Chem. Kinet.*, 1988, **20**, 41.
- 28 T. J. Wallington, J. M. Andino, L. M. Skewes, W. O. Siegl and S. M. Japar, *Int. J. Chem. Kinet.*, 1989, **21**, 993.
- 29 L. Nelson, O. Rattigan, R. Neavyn, H. Sidebottom, J. Treacy and O. J. Nielsen, *Int. J. Chem. Kinet.*, 1990, **22**, 1111.
- 30 M. Semadeni, D. W. Stocker and J. A. Kerr, *J. Atmos. Chem.*, 1993, **16**, 79.
- 31 A. Mellouki, S. Teton and G. LeBras, *Int. J. Chem. Kinet.*, 1995, **27**, 791.
- 32 F. Kramp and S. E. Paulson, *J. Phys. Chem. A*, 1998, **102**, 2685.
- 33 R. Volkamer, K. H. Becker, B. Klotz, U. Platt, J. Uecker and K. Wirtz, in *Proceedings of the "Workshop on the Chemical Behaviour of Aromatic Hydrocarbons in the Troposphere"*, ed. K. H. Becker, Bergische Universität Wuppertal, <http://www.physchem.uni-wuppertal.de/PC-WWW-Site/workshops.html>, Valencia, Spain, February 27–29, 2000, p. 15.
- 34 R. Volkamer, U. Platt, J. Uecker and K. Wirtz, in *EUPHORE annual report 1998–1999*, ed. I. Barnes and K. J. Brockmann, Bergische Universität Wuppertal, 2001, p. 278.
- 35 M. Semadeni, D. W. Stocker and J. A. Kerr, *Int. J. Chem. Kinet.*, 1995, **27**, 287.
- 36 B. Bohn, M. Elend and C. Zetzsch, Report TFS Teilprojekt LT3-D3, 1999.
- 37 B. Trost, J. Stutz and U. Platt, *Atmos. Environ.*, 1997, **31**, 3999.
- 38 T. Berndt, O. Böge and H. Herrmann, *Chem. Phys. Lett.*, 1999, **314**, 435.
- 39 T. Berndt, 2000, *personal communication*.
- 40 J. Mellqvist and A. Rosén, *J. Quant. Spectrosc. Radiat. Transfer*, 1996, **56**, 209.
- 41 *In situ EUPHORE Radical Measurement, EUPHORAM*, ed. K. H. Becker, Final Report of the EC project, Contract ENV4-CT95-0011, Bergische Universität Wuppertal, 1999.
- 42 B. Klotz, I. Barnes and K. H. Becker, *Chem. Phys.*, 1998, **231**, 289.
- 43 B. Klotz, A. Bierbach, I. Barnes and K. H. Becker, *Environ. Sci. Technol.*, 1995, **29**, 2322.
- 44 W. P. L. Carter, A. Winer and J. N. Pitts, Jr., *Environ. Sci. Technol.*, 1981, **15**, 829.
- 45 R. Volkamer, Dissertation, University of Heidelberg, <http://archiv.ub.uni-heidelberg.de>, 2001.
- 46 A. Geyer, B. Alicke, S. Konrad, T. Schmitz, J. Stutz and U. Platt, *J. Geophys. Res.*, 2001, **106**, **D8**, 8013–8025.
- 47 R. Ackermann, K. H. Becker, A. Geyer, J. A. G. Gomes, R. Kurtenbach, J. C. Lörzer and U. Platt, in *Proceedings of the "Workshop on the Chemical Behaviour of Aromatic Hydrocarbons in the Troposphere"*, ed. K. H. Becker, Bergische Universität Wuppertal, <http://www.physchem.uni-wuppertal.de/PC-WWW-Site/workshops.html>, Valencia, Spain, February 27–29, 2000, p. 124.
- 48 R. Kurtenbach, R. Ackermann, K.H. Becker, A. Geyer, J.A.G. Gomes, J.C. Lörzer, U. Platt and P. Wiesen, *J. Phys. Chem.*, 2002.
- 49 U. Brandenburger, T. Brauers, H.P. Dorn, M. Hausmann and D.H. Ehhalt, *J. Atmos. Chem.*, 1998, **31**(1–2), 181.
- 50 R. Volkamer, U. Platt, J. Uecker and K. Wirtz, in *EUPHORE annual report 1998–1999*, ed. I. Barnes and K. J. Brockmann, Bergische Universität Wuppertal, 2001, p. 257.
- 51 M. Jenkin, S. M. Saunders and R. G. Derwent, in *Proceedings of the "Workshop on the Chemical Behaviour of Aromatic Hydrocarbons in the Troposphere"*, ed. K. H. Becker, Bergische Universität Wuppertal, <http://www.physchem.uni-wuppertal.de/PC-WWW-Site/workshops.html>, Valencia, Spain, February 27–29, 2000, p. 81.
- 52 D. F. Smith, C. McIver and T. Kleindienst, *J. Atmos. Chem.*, 1998, **30**, 209.
- 53 D. F. Smith, T. Kleindienst and C. McIver, *J. Atmos. Chem.*, 1999, **34**, 339.